KIAS-P16073

A testable radiative neutrino mass model without additional symmetries and Explanation for the $b \to s\ell^+\ell^-$ anomaly

Kingman Cheung,[1,2,3,*] Takaaki Nomura,[4,†] and Hiroshi Okada[1,‡]

[1]*Physics Division, National Center for Theoretical Sciences, Hsinchu, Taiwan 300*

[2]*Department of Physics, National Tsing Hua University, Hsinchu 300, Taiwan*

[3]*Division of Quantum Phases and Devices, School of Physics, Konkuk University, Seoul 143-701, Republic of Korea*

[4]*School of Physics, KIAS, Seoul 130-722, Korea*

(Dated: December 13, 2016)

We propose a one-loop radiative Majorana-type neutrino-mass matrix without any kind of additional symmetries by introducing two leptoquark-like bosons only. In this scenario, we show that the anomaly appearing in the process $b \to s\ell\bar{\ell}$ can be explained without any conflicts against various constraints such as lepton-flavor violations, flavor-changing neutral currents, oblique parameters ΔS, ΔT, and the Drell-Yan process. We make the predictions for the flavor-violating lepton-pair production ($e\mu$, $e\tau$, and $\mu\tau$) at the LHC, as well as the cross sections for pair production of these leptoquark-like bosons.

arXiv:1610.02322v3 [hep-ph] 12 Dec 2016

I. INTRODUCTION

The standard model (SM) of particle physics is so successful that all the experiments searching for signs beyond the SM resulted in negative results and the SM has been tested to a precision of 10^{-3}. Yet, the neutrino oscillation experiments accumulated enough evidences that the neutrinos do have masses. Massive neutrinos are then the only formally established

*Electronic address: cheung@phys.nthu.edu.tw

†Electronic address: nomura@kias.re.kr

‡Electronic address: macokada3hiroshi@cts.nthu.edu.tw

evidences beyond the SM. Although there are some other observations which also point to physics beyond the SM, such as existence of dark matter, accelerated expansion of the Universe, and matter-antimatter asymmetry, however, they are not as convincing as the massive neutrinos.

Extensions or modifications of the SM are often put forward to explain the neutrino masses and their oscillation patterns. The most celebrated one is the see-saw mechanism with the introduction of heavy right-handed (RH) neutrinos at the mass scale of 10^{11-12} GeV [1]. There are variations in the see-saw type models with TeV RH neutrinos [2]. The advantage of TeV see-saw models is that they can be tested in the LHC experiments [3]. Another type of neutrino mass models is based on loop diagrams, in which the small neutrino mass is naturally obtained by the suppression loop factor. Some classic examples are the one-loop Zee model [4] and Ma model [5], two-loop Zee-Babu model [6], three-loop Krauss-Nasri-Trodden model [7], etc. Often in this type of models, some ad hoc symmetries are introduced to forbid some unwanted contributions or the see-saw contributions if there are RH neutrinos in the model.

Recently, there was an 2.6σ anomaly in lepton-universality violation measured in the ratio $R_K \equiv B(B \to K\mu\mu)/B(B \to Kee) = 0.745^{+0.090}_{-0.074} \pm 0.036$ by LHCb [8]. Also, sizable deviations from the SM prediction were recorded in angular distributions of $B \to K^*\mu\mu$ [9]. The results can be accounted for by a large negative contribution to the Wilson coefficient C_9 of the semileptonic operator O_9, and also contributions to other Wilson coefficients, in particular to C_9' [10–12].

Here we propose a simple extensions of the SM with introduction of a color-triplet $SU(2)_L$-doublet scalar boson η and a color-antitriplet $SU(2)_L$-triplet scalar boson Δ without assuming further discrete or gauge symmetries. The $SU(3)_C$, $SU(2)_L$, $U(1)_Y$ quantum numbers of the new fields are summarized in Table I. We shall show that this model can successfully explain the neutrino masses and the oscillation pattern, as well as solving the anomalies in $b \to s\ell\bar{\ell}$ with additional contributions to $C_{9,10}$ and $C'_{9,10}$, and at the same time satisfying all the existing constraints of lepton-flavor violations (LFV), flavor-changing neutral currents (FCNC), and S, T, U parameters. Furthermore, the masses of η and Δ bosons are in the TeV scale, and so can be tested in the Drell-Yan process and lepton-flavor violating production, and also directly in the pair production via the $\ell\ell jj$ final state. This is the main result of the work.

	η	Δ
$SU(3)_C$	**3**	$\bar{\mathbf{3}}$
$SU(2)_L$	**2**	**3**
$U(1)_Y$	$\frac{1}{6}$	$\frac{1}{3}$

TABLE I: Charge assignments of the new fields η and Δ under $SU(3)_C \times SU(2)_L \times U(1)_Y$.

This paper is organized as follows. In Sec. II, we review the model and describe the constraints. In Sec. III, we analyze numerically the parameter space so as to solve the anomaly in $b \to s\ell\ell$, and calculate the cross sections for lepton-flavor violating production. We conclude in Sec. IV.

II. MODEL SETUP AND CONSTRAINTS

The new field contents and their charges are shown in Table I, in which the color-triplet η is an $SU(2)_L$ doublet with 1/6 hypercharge, while the color-antitriplet Δ is an $SU(2)_L$ triplet with 1/3 hypercharge. The relevant Lagrangian for the interactions of the η and Δ with fermions and the Higgs field is given by

$$-\mathcal{L}_Y = f_{ij}\overline{d_{R_i}}\tilde{\eta}^\dagger L_{L_j} + g_{ij}\overline{Q^c_{L_i}}(i\sigma_2)\Delta L_{L_j} - \mu\Phi^\dagger\Delta\eta + \text{h.c.}, \tag{II.1}$$

where $(i,j) = 1-3$ are generation indices, $\tilde{\eta} \equiv i\sigma_2\eta^*$, σ_2 is the second Pauli matrix, and Φ is the SM Higgs field that develops a nonzero vacuum expectation value (VEV), which is symbolized by $\langle\Phi\rangle \equiv v/\sqrt{2}$. We work in the basis where all the coefficients are real and positive for simplicity. The scalar fields can be parameterized as

$$\Phi = \begin{bmatrix} w^+ \\ \frac{v+\phi+iz}{\sqrt{2}} \end{bmatrix}, \quad \eta = \begin{bmatrix} \eta_{2/3} \\ \eta_{-1/3} \end{bmatrix}, \quad \Delta = \begin{bmatrix} \frac{\delta_{1/3}}{\sqrt{2}} & \delta_{4/3} \\ \delta_{-2/3} & -\frac{\delta_{1/3}}{\sqrt{2}} \end{bmatrix}, \tag{II.2}$$

where the subscript of the fields represents the electric charge, $v \approx 246$ GeV, and $w^\pm$ and z are, respectively, the Nambu-Goldstone bosons, which will then be absorbed by the longitudinal component of the W and Z bosons. Due to the μ term in Eq. (II.1), the charged components with 1/3 and 2/3 electric charges mix, such that their mixing matrices and mass

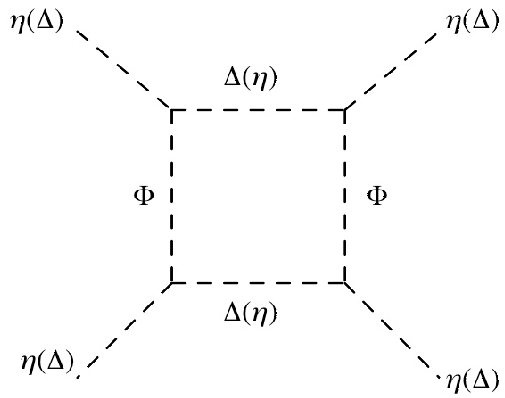

FIG. 1: One-loop diagrams for estimating the constraint from vacuum stability.

eigenstates are defined as follows:

$$\begin{bmatrix} \eta_{i/3} \\ \delta_{i/3} \end{bmatrix} = O_i \begin{bmatrix} A_i \\ B_i \end{bmatrix}, \quad O_i \equiv \begin{bmatrix} c_{\alpha_i} & s_{\alpha_i} \\ -s_{\alpha_i} & c_{\alpha_i} \end{bmatrix}, \quad (i = 1, 2), \tag{II.3}$$

where their masses are denoted as m_{A_i} and m_{B_i} respectively. The interactions in terms of the mass eigenstates can be written as

$$-L_Y \approx f_{ij}\overline{d_{R_i}}\nu_{L_j}(c_{\alpha_1}A_1 + s_{\alpha_1}B_1) - \frac{g_{ij}}{\sqrt{2}}\overline{d^c_{L_i}}\nu_{L_j}(-s_{\alpha_1}A_1 + c_{\alpha_1}B_1) \tag{II.4}$$

$$- f_{ij}\overline{d_{R_i}}\ell_{L_j}(c_{\alpha_2}A_2 + s_{\alpha_2}B_2) - \frac{g_{ij}}{\sqrt{2}}\overline{u^c_{L_i}}\ell_{L_j}(-s_{\alpha_1}A_1 + c_{\alpha_1}B_1) \tag{II.5}$$

$$- g_{ij}\overline{d^c_{L_i}}\ell_{L_j}\delta_{4/3} \; + \; g_{ij}\overline{u^c_{L_i}}\nu_{L_j}(-s_{\alpha_2}A_2^* + c_{\alpha_2}B_2^*). \tag{II.6}$$

Vacuum stability: Since we have charged components such as $\eta_{1/3,2/3}$ and $\delta_{1/3,2/3,4/3}$, we have to avoid their pure couplings from becoming negative by restricting the negative contribution at one-loop level due to the μ term to be smaller than the tree-level coupling. Estimating the one-loop diagrams in Fig. 1, these conditions are respectively given by

$$\frac{\mu^4}{2(4\pi)^2}\int \frac{dxdy\delta(x+y-1)xy}{(xm_\Phi^2 + ym_\delta^2)^2} \lesssim \lambda_\eta^{\rm tree}, \quad \frac{\mu^4}{2(4\pi)^2}\int \frac{dxdy\delta(x+y-1)xy}{(xm_\Phi^2 + ym_\eta^2)^2} \lesssim \lambda_\delta^{\rm tree}, \tag{II.7}$$

where $m_{\eta/\delta}$ are the bare masses in the potential. Now we estimate the typical upper bound of μ, assuming $m_{\eta/\delta} \approx 1$ TeV that comes from collider bounds as shall be seen later. Also, we restrict $\lambda_{\eta/\delta}^{\rm tree} \lesssim 4\pi$. Under the framework, one obtains $|\mu| \lesssim 6.4$ TeV, which gives almost no constraint on the TeV scale model. Thus, we do not need to worry about the stability condition.

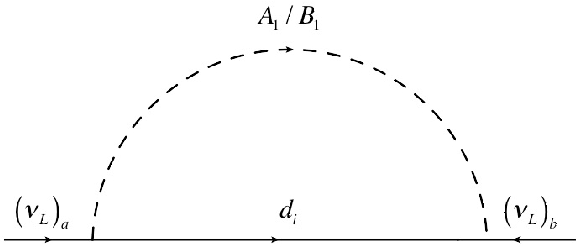

FIG. 2: One-loop diagrams for generating the neutrino mass matrix.

A. Neutrino mixing

The dominant contribution to the active neutrino mass matrix m_ν is given at one-loop level through interactions in Eq. (II.4) as illustrated in Fig. 2, and its formula is given by

$$(m_\nu)_{ab} = \frac{N_c s_{\alpha_1} c_{\alpha_1}}{2(4\pi)^2}\left[1 - \frac{m_{A_1}^2}{m_{B_1}^2}\right]\sum_{i=1}^{3}\left[g_{bi}^T m_{d_i} f_{ia} + f_{ai} m_{d_i} g_{ib}^T\right] F_I(r_{A_1}, r_{m_{d_i}}), \tag{II.8}$$

$$F_I(r_1, r_2) = \frac{r_1(r_2-1)\ln r_1 - r_2(r_1-1)\ln r_2}{(r_1-1)(r_2-1)(r_1-r_2)}, \quad (r_1 \neq 1), \tag{II.9}$$

where $N_c = 3$ is the color factor and we define $r_f \equiv (m_f/m_{B_i})^2$. $(m_\nu)_{ab}$ is diagonalized by the Pontecorvo-Maki-Nakagawa-Sakata mixing matrix $V_{\rm MNS}$ (PMNS) [13] as $(m_\nu)_{ab} = (V_{\rm MNS} D_\nu V_{\rm MNS}^T)_{ab}$ with $D_\nu \equiv (m_{\nu_1}, m_{\nu_2}, m_{\nu_3})$, where we use the data in the global analysis [14]. Then one can parameterize as

$$g^T R f \equiv \frac{1}{2}\left[V_{\rm MNS} D_\nu V_{\rm MNS}^T + A\right], \quad R \equiv \frac{N_c s_{\alpha_1} c_{\alpha_1}}{2(4\pi)^2}\left[1 - \frac{m_{A_1}^2}{m_{B_1}^2}\right]\sum_{i=1}^{3} m_{d_i} F_I(r_{A_1}, r_{m_{d_i}}), \tag{II.10}$$

where A is an arbitrary antisymmetric matrix with complex values. Finally, we derive the following relations [15]:

$$g = \frac{1}{2}(V_{\rm MNS}^* D_\nu V_{\rm MNS}^\dagger + A) f^{-1} R^{-1}, \text{ or } f = \frac{1}{2} R^{-1} (g^T)^{-1} (V_{\rm MNS}^* D_\nu V_{\rm MNS}^\dagger + A). \tag{II.11}$$

In the numerical analysis, we shall use the former relation for convenience.

B. LFVs and FCNCs at tree level

Leptoquark models often induce LFVs and FCNCs at tree level. Several processes can arise from the terms g and f and these processes can be estimated by the effective Hamil-

tonian [16] as

$$(\mathcal{H}_{\rm eff})^{\bar{\ell}\ell\bar{d}d}_{ijkn} = f_{kj}f^{\dagger}_{in}\left(\frac{c^2_{\alpha_2}}{m^2_{A_2}}+\frac{s^2_{\alpha_2}}{m^2_{B_2}}\right)(\bar{\ell}_i\gamma^\mu P_L\ell_j)(\bar{d}_k\gamma_\mu P_R d_n) - \frac{g_{kj}g^{\dagger}_{in}}{m^2_\delta}(\bar{\ell}_i\gamma^\mu P_L\ell_j)(\bar{d}_k\gamma_\mu P_L d_n)$$
$$\equiv C^{\bar{\ell}\ell\bar{d}d}_{LR}(\bar{\ell}_i\gamma^\mu P_L\ell_j)(\bar{d}_k\gamma_\mu P_R d_n) + C^{\bar{\ell}\ell\bar{d}d}_{LL}(\bar{\ell}_i\gamma^\mu P_L\ell_j)(\bar{d}_k\gamma_\mu P_L d_n), \quad \text{(II.12)}$$

$$(\mathcal{H}_{\rm eff})^{\bar{\ell}\ell\bar{u}u}_{ijkn} = -\frac{g_{kj}g^{\dagger}_{in}}{2}\left(\frac{s^2_{\alpha_1}}{m^2_{A_1}}+\frac{c^2_{\alpha_1}}{m^2_{B_1}}\right)(\bar{\ell}_i\gamma^\mu P_L\ell_j)(\bar{u}_k\gamma_\mu P_L u_n)$$
$$\equiv C^{\bar{\ell}\ell\bar{u}u}_{LL}(\bar{\ell}_i\gamma^\mu P_L\ell_j)(\bar{u}_k\gamma_\mu P_L u_n), \quad \text{(II.13)}$$

$$(\mathcal{H}_{\rm eff})^{\bar{\nu}\nu\bar{q}q}_{ijkn} = -\frac{g_{kj}g^{\dagger}_{in}}{2}\left(\frac{s^2_{\alpha_1}}{m^2_{A_1}}+\frac{c^2_{\alpha_1}}{m^2_{B_1}}\right)(\bar{\nu}_i\gamma^\mu P_L\nu_j)(\bar{q}_k\gamma_\mu P_L q_n)$$
$$\equiv C^{\bar{\nu}\nu\bar{q}q}_{LL}(\bar{\nu}_i\gamma^\mu P_L\nu_j)(\bar{q}_k\gamma_\mu P_L q_n). \quad \text{(II.14)}$$

Then one can rewrite the relevant coefficients as

$$\epsilon^{\bar{\ell}\ell\bar{d}d}_{ijkn} = \frac{\sqrt{2}}{4{\rm G_F}}(C^{\bar{\ell}\ell\bar{d}d}_{LR}+C^{\bar{\ell}\ell\bar{d}d}_{LL}), \quad \text{(II.15)}$$

$$\epsilon^{\bar{\ell}\ell\bar{u}u}_{ijkn} = \frac{\sqrt{2}}{4{\rm G_F}}C^{\bar{\ell}\ell\bar{u}u}_{LL}, \quad \text{(II.16)}$$

$$\epsilon^{\bar{\nu}\nu\bar{q}q}_{ijkn} = \frac{\sqrt{2}}{4{\rm G_F}}C^{\bar{\nu}\nu\bar{q}q}_{LL}, \quad \text{(II.17)}$$

where the experimental bounds on each coefficient are summarized in Tables II, III, and IV [16].

$B_{d/s} \to \mu^+\mu^-$ measurements: Recently, CMS [17] and LHCb [18] experiments reported the branching ratios of $B(B_s \to \mu^+\mu^-)$ and $B(B_d \to \mu^+\mu^-)$, which can place interesting bounds on new physics. The bounds on the coefficients of the effective Hamiltonians in Eq. (II.12) [19] are

$$B(B_s \to \mu^+\mu^-): \quad 0 \lesssim |C^{\bar{\mu}\mu\bar{s}b}_{LR}+C^{\bar{\mu}\mu\bar{s}b}_{LL}| \lesssim 5\times10^{-9}\ {\rm GeV}^{-2}, \quad \text{(II.18)}$$

$$B(B_d \to \mu^+\mu^-): \quad 1.5\times10^{-9}\ {\rm GeV}^{-2} \lesssim |C^{\bar{\mu}\mu\bar{d}b}_{LR}+C^{\bar{\mu}\mu\bar{d}b}_{LL}| \lesssim 3.9\times10^{-9}\ {\rm GeV}^{-2}, \quad \text{(II.19)}$$

where the phase is assumed to be zero for simplicity. The bounds from the other modes are

$$B(B_s \to e^+e^-): \quad |C^{\bar{e}e\bar{s}b}_{LR}+C^{\bar{e}e\bar{s}b}_{LL}| \lesssim 2.54\times10^{-5}\ {\rm GeV}^{-2}, \quad \text{(II.20)}$$

$$B(B_d \to e^+e^-): \quad |C^{\bar{e}e\bar{d}b}_{LR}+C^{\bar{e}e\bar{d}b}_{LL}| \lesssim 1.73\times10^{-5}\ {\rm GeV}^{-2}, \quad \text{(II.21)}$$

$$B(B_s \to \tau^+\tau^-): \quad |C^{\bar{\tau}\tau\bar{s}b}_{LR}+C^{\bar{\tau}\tau\bar{s}b}_{LL}| \lesssim 1.2\times10^{-8}\ {\rm GeV}^{-2}, \quad \text{(II.22)}$$

$$B(B_d \to \tau^+\tau^-): \quad |C^{\bar{\tau}\tau\bar{d}b}_{LR}+C^{\bar{\tau}\tau\bar{d}b}_{LL}| \lesssim 1.28\times10^{-6}\ {\rm GeV}^{-2}. \quad \text{(II.23)}$$

$ijkn$ of $\epsilon^{\bar{\ell}\ell\bar{d}d}_{ijkn}$	Constraints on $\epsilon^{\bar{\ell}\ell\bar{d}d}_{ijkn}$	Observable	Experimental value
$eeds(\to 1112)$	5.7×10^{-5}	$B(K_L^0\to\bar{e}e)$	9.0×10^{-12}
$eedb(\to 1113)$	2.0×10^{-4}	$\frac{B(B^+\to\pi^+\bar{e}e)}{B(B^0\to\pi^-\bar{e}\nu_e)}$	$<\frac{1.8\times10^{-7}}{1.34\times10^{-4}}$
$eesb(\to 1123)$	1.8×10^{-4}	$\frac{B(B^+\to K^+\bar{e}e)}{B(B^0\to D^0\bar{e}\nu_e)}$	$\frac{4.9\times10^{-7}}{2.2\times10^{-2}}$
$e\mu dd(\to 1211)$	8.5×10^{-7}	$\mu-e$ conversion on Ti	$\frac{\sigma(\mu^-Ti\to e^-Ti)}{\sigma(\mu^-Ti\to capture)}<4.3\times10^{12}$
$e\mu ds(\to 1212)$	3.0×10^{-7}	$B(K_L^0\to\bar{e}\mu)$	$<4.7\times10^{-12}$
$e\mu db(\to 1213)$	2.0×10^{-4}	$\frac{B(B^+\to\pi^+\bar{e}\mu)}{B(B^0\to\pi^-\bar{e}\nu_e)}$	$\frac{1.7\times10^{-7}}{1.34\times10^{-4}}$
$e\mu sb(\to 1223)$	8×10^{-5}	$\frac{B(B^+\to K^+\bar{e}\mu)}{B(B^+\to D^0\bar{e}\nu_e)}$	$<\frac{9.1\times10^{-8}}{2.2\times10^{-2}}$
$e\tau dd(\to 1311)$	8.4×10^{-4}	$\frac{B(\tau\to\pi^0e)}{B(\tau\to\pi\nu_\tau)}$	$<\frac{8\times10^{-8}}{10.91\times10^{-2}}$
$e\tau ds(\to 1312)$	4.9×10^{-4}	$\frac{B(\tau\to eK)}{B(\tau\to\bar{\nu}K)}$	$B<3.3\times10^{-8}$
$e\tau db(\to 1313)$	4.1×10^{-3}	$B(B^0\to\bar{e}\tau)$	$<1.1\times10^{-4}$
$\mu\mu ds(\to 2212)$	7.8×10^{-6}	$B(K_L^0\to\bar{\mu}\mu)$	6.84×10^{-9}
$\mu\mu db(\to 2213)$	1.3×10^{-4}	$\frac{B(B^+\to\pi^+\bar{\mu}\mu)}{B(B^0\to\pi^-\bar{e}\nu_e)}$	$<\frac{6.9\times10^{-8}}{1.3\times10^{-4}}$
$\mu\tau dd(\to 2311)$	9.8×10^{-4}	$\frac{B(\tau\to\pi^0\mu)}{B(\tau\to\pi^-\nu_\tau)}$	$<\frac{1.1\times10^{-7}}{10.91\times10^{-2}}$
$\mu\tau ds(\to 2312)$	5.4×10^{-4}	$\frac{B(\tau\to\mu K)}{B(\tau\to\bar{\nu}K)}$	$B<4.0\times10^{-8}$
$\mu\tau db(\to 2313)$	2.1×10^{-2}	$B(B^0\to\bar{\mu}\tau)$	$<2.2\times10^{-5}$
$\mu\tau sb(\to 2323)$	2.3×10^{-3}	$\frac{B(B^+\to K^+\bar{\tau}\mu)}{B(B^+\to D^0\bar{e}\nu)}$	$<\frac{7.7\times10^{-5}}{2.2\times10^{-2}}$
$\tau\tau db(\to 3313)$	0.2	$B(B^0\to\bar{\tau}\tau)$	$<4.1\times10^{-3}$

TABLE II: Summary for the experimental bounds on $\epsilon^{\bar{\ell}\ell\bar{d}d}_{ijkn}$.

C. LFVs and FCNCs at the one-loop level

LFVs: $\ell_a\to\ell_b\gamma$ processes, which arise from Eqs. (II.5) and (II.6) via one-loop diagrams as shown in Fig. 3, often give stringent experimental constraints, and the branching ratio is given by

$$B(\ell_a\to\ell_b\gamma)=\frac{48\pi^3C_a\alpha_{\rm em}}{\mathrm{G_F^2}m_a^2}(|(a_R)_{ab}|^2+|(a_L)_{ab}|^2), \tag{II.24}$$

$ijkn$ of $\epsilon^{\bar{\ell}\ell\bar{u}u}_{ijkn}$	Constraints on $\epsilon^{\bar{\ell}\ell\bar{u}u}_{ijkn}$	Observable	Experimental value
$eeuc(\to 1112)$	7.9×10^{-3}	$\frac{B(D^+\to\pi^+\bar{e}e)}{B(D^0\to\pi^-\bar{e}\nu_e)}$	$<\frac{7.4\times10^{-6}}{2.83\times10^{-3}}$
$eett(\to 1133)$	0.092	$Z\to\bar{e}e$	$R_e=20.804\pm0.050$
$e\mu uu(\to 1211)$	8.5×10^{-7}	$\mu-e$ conversion on Ti	$\frac{\sigma(\mu Ti\to eTi)}{\sigma(\mu Ti\to capture)}<4.3\times10^{-12}$
$e\mu uc(\to 1212)$	1.7×10^{-2}	$\frac{B(D^+\to\pi^+\bar{e}\mu)}{B(D^0\to\pi^-\bar{e}\nu_e)}$	$<\frac{3.4\times10^{-5}}{2.83\times10^{-3}}$
$e\mu tt(\to 1233)$	0.1	$Z\to\bar{e}\mu$	$B<1.7\times10^{-6}$
$e\tau uu(\to 1311)$	8.4×10^{-4}	$\frac{B(\tau\to\pi^0e)}{B(\tau\to\pi^-\nu_\tau)}$	$<\frac{8\times10^{-8}}{10.91\times10^{-2}}$
$e\tau tt(\to 1233)$	0.2	$Z\to\bar{e}\tau$	$B<9.8\times10^{-6}$
$\mu\mu uc(\to 2212)$	6.1×10^{-3}	$\frac{B(D^+\to\pi^+\bar{\mu}\mu)}{B(D^0\to\pi^-\bar{e}\nu_e)}$	$<\frac{3.9\times10^{-6}}{2.83\times10^{-3}}$
$\mu\mu tt(\to 2233)$	0.061	$Z\to\bar{\mu}\mu$	$R_\mu=20.785\pm0.033$
$\mu\tau uu(\to 2311)$	9.8×10^{-4}	$\frac{B(\tau\to\pi^0\mu)}{B(\tau\to\pi^-\nu_\tau)}$	$<\frac{1.1\times10^{-7}}{10.91\times10^{-2}}$
$\mu\tau tt(\to 2333)$	1	$Z\to\tau\bar{\mu}$	$B<12\times10^{-6}$
$\tau\tau tt(\to 3333)$	0.086	$Z\to\bar{\tau}\tau$	$R_\tau=20.764\pm0.045$

TABLE III: Summary for the experimental bounds on $\epsilon^{\bar{\ell}\ell\bar{u}u}_{ijkn}$.

$ijkn$ of $\epsilon^{\bar{\nu}_i\nu_j\bar{q}_kq_n}_{ijkn}$	Constraints on $\epsilon^{\bar{\nu}_i\nu_j\bar{q}_kq_n}_{ijkn}$	Observable	Experimental value
$ijds(\to ij12)$	9.4×10^{-6}	$\frac{B(K^+\to\pi^+\bar{\nu}\nu)}{B(K^+\to\pi^0\bar{e}\nu_e)}$	$\frac{1.5\times10^{-10}}{5.08\times10^{-2}}$

TABLE IV: Summary for the experimental bounds on $\epsilon^{\bar{\nu}_i\nu_j\bar{q}_kq_n}_{ijkn}$, where $(i,j)=(1-3)$.

where $m_{a(b)}$ is the mass for the charged-lepton eigenstate, $C_a=(1,1/5)$ for $(a=\mu,\tau)$. a_L and a_R are respectively given by

$$\frac{(a_R)_{ab}}{N_c}\approx-\frac{f^\dagger_{bi}f_{ia}m_a}{12(4\pi)^2}\left(\left[\frac{Q_{A_2}c^2_{\alpha_2}}{m^2_{A_2}}+\frac{Q_{B_2}s^2_{\alpha_2}}{m^2_{B_2}}\right]+2\left[\frac{Q_dc^2_{\alpha_2}}{m^2_{A_2}}+\frac{Q_ds^2_{\alpha_2}}{m^2_{B_2}}\right]\right) \tag{II.25}$$
$$+\frac{g^\dagger_{bi}g_{ia}m_a}{24(4\pi)^2}\left(\left[\frac{-Q_\delta}{m^2_\delta}+\frac{2Q_{\bar{d}}}{m^2_\delta}\right]-\left[\frac{Q_{A_1}s^2_{\alpha_1}}{m_{A_1}}+\frac{Q_{B_1}c^2_{\alpha_1}}{m_{B_1}}\right]+2Q_{\bar{u}}\left[\frac{s^2_{\alpha_1}}{m_{A_1}}+\frac{c^2_{\alpha_1}}{m_{B_1}}\right]\right),$$

where we have assumed $m_{d(u)}<<m_{A_i,B_i,\delta}(i=1-2)$, and $a_L=a_R(m_a\to m_b)$, $Q_\delta=-Q_{\bar{\delta}}\equiv-4/3$, $Q_{A_2}=Q_{B_2}\equiv-2/3$, $Q_{A_1}=Q_{B_1}\equiv-1/3$, $Q_d=-Q_{\bar{d}}\equiv-1/3$, $Q_u=-Q_{\bar{u}}\equiv2/3$. The current experimental upper bounds are given by [20, 21]

$$B(\mu\to e\gamma)\le4.2\times10^{-13},\quad B(\tau\to\mu\gamma)\le4.4\times10^{-8},\quad B(\tau\to e\gamma)\le3.3\times10^{-8}\ . \tag{II.26}$$

The muon anomalous magnetic moment (muon $g-2$): It has been measured with a high precision, and its deviation from the SM prediction is of order 10^{-9}. The formula for the

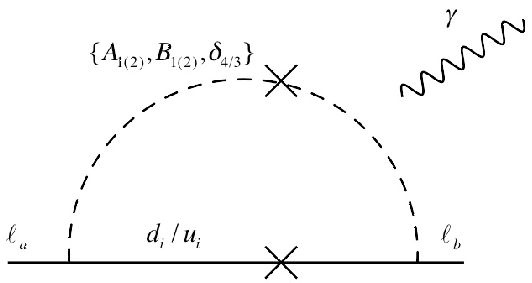

FIG. 3: One-loop diagrams for the LFV processes $\ell_a \to \ell_b\gamma$ where the cross mark on the internal lines indicates the attachment of a photon line.

muon $g-2$ is given by

$$\Delta a_\mu \approx -m_\mu[(a_R)_{22} + (a_L)_{22}]. \tag{II.27}$$

In our model, typical values are at most 10^{-14} with mostly the negative sign. Although there may exist some positive sources, however, the negative sources are always larger than the positive ones when we impose all the bounds from LFVs and FCNCs.

$Q-\overline{Q}$ *mixing*: We also consider the constraint of the $Q-\overline{Q}$ mixing, where $Q = K, B, D$. The mixing is characterized by Δm_Q given by [22]

$$\Delta m_K \approx \sum_{i,j=1}^{3} \frac{5 f_K^2 m_K^3 \left(8 f_{i2}^\dagger f_{1i} f_{1j} f_{j2}^\dagger m_{B_1}^2 m_\delta^2 + g_{2i} g_{i1}^\dagger g_{2j} g_{j1}^\dagger (4m_{B_1}^2 + m_\delta^2)\right)}{768\pi^2 m_{A_1}^2 m_{B_1}^2 m_\delta^2 (m_d + m_s)^2} \lesssim 3.48 \times 10^{-15}[\text{GeV}], \tag{II.28}$$

$$\Delta m_B \approx \sum_{i,j=1}^{3} \frac{5 f_B^2 m_B^3 \left(8 f_{i2}^\dagger f_{3i} f_{3j} f_{j2}^\dagger m_{B_1}^2 m_\delta^2 + g_{2i} g_{i3}^\dagger g_{2j} g_{j3}^\dagger (4m_{B_1}^2 + m_\delta^2)\right)}{768\pi^2 m_{A_1}^2 m_{B_1}^2 m_\delta^2 (m_b + m_s)^2} \lesssim 3.36 \times 10^{-13}[\text{GeV}], \tag{II.29}$$

$$\Delta m_D \approx \sum_{i,j=1}^{3} \frac{5 f_D^2 m_D^3 g_{2i} g_{i1}^\dagger g_{2j} g_{j1}^\dagger}{768\pi^2 m_{B_1}^2 (m_u + m_c)^2} \lesssim 6.25 \times 10^{-15}[\text{GeV}],, \tag{II.30}$$

where we assume $m_{A_1} \approx m_{A_2}$, $m_{B_1} \approx m_{B_2}$, and $s_{\alpha_{1(2)}} \approx 0$, and each of the last inequalities of Eqs.(II.28, II.30) represents the upper bound on the experimental values [23], and $f_K \approx 0.156$ GeV, $f_B \approx 0.191$ GeV, $m_K \approx 0.498$ GeV, and $m_B \approx 5.280$ GeV.

$b \to s\gamma$: It can arise from the same term in the LFVs, yet the constraint is always weaker than those of LFVs. Thus we do not further consider this process.

D. Oblique parameters

Since η and Δ are multiplets under the $SU(2)_L$ gauge symmetry, we need to take into account the constraints from the oblique parameters S, T, and U. Here we focus on the new physics contributions to S and T parameters, ΔS and ΔT, which are defined by

$$\Delta S = 16\pi \frac{d}{dq^2}[\Pi_{33}(q^2) - \Pi_{3Q}(q^2)]|_{q^2\to 0}, \quad \Delta T = \frac{16\pi}{s_W^2 m_Z^2}[\Pi_{\pm}(0) - \Pi_{33}(0)], \tag{II.31}$$

where $s_W^2 \approx 0.22$ is the Weinberg angle and m_Z is the Z boson mass. The loop factors $\Pi_{33,3Q,QQ,\pm}(q^2)$ are calculated from the one-loop vacuum-polarization diagrams for Z and $W^\pm$ bosons, $i\Pi^{\mu\nu}_{Z(W)}$, where new particles run inside the loop diagrams, as follows;

$$\Pi^{\mu\nu}_Z = g^{\mu\nu}\frac{e^2}{c_W^2 s_W^2}\left(\Pi_{33}(q^2) - 2s_W^2\Pi_{3Q}(q^2) - s_W^4\Pi_{QQ}(q^2)\right), \tag{II.32}$$

$$\Pi^{\mu\nu}_W = g^{\mu\nu}\frac{e^2}{s_W^2}\Pi_{\pm}(q^2), \tag{II.33}$$

The list of new particle contributions is quite lengthy and so we summarize them in the Appendix. The experimental bounds are given by [23]

$$(0.05 - 0.09) \le \Delta S \le (0.05 + 0.09), \quad (0.08 - 0.07) \le \Delta T \le (0.08 + 0.07). \tag{II.34}$$

E. Collider physics

The interactions of the η and Δ are very similar to leptoquarks or squarks. The first signature that we consider is their effects on Drell-Yan production and also the lepton-flavor violating production processes such as $e^\pm\mu^\mp$, $\mu^\pm\tau^\mp$, and $e^\pm\tau^\mp$ [24].

Without loss of generality we take the mixing angles between η and Δ to be small (indeed required by the S, T parameters), such that $\eta_{1/3,2/3} \approx A_{1,2}$ and $\delta_{1/3,2/3} \approx B_{1,2}$. We can write down the amplitude for $d_{R_i}(p_1)\overline{d_{R_{i'}}}(p_2) \to \ell_{L_j}(q_1)\bar{\ell}_{L_{j'}}(q_2)$ with a t-channel exchange of $\eta_{2/3}$

$$\begin{aligned} i\mathcal{M} &= -if_{ij}f_{i'j'}\frac{1}{\hat{t} - m_\eta^2}\bar{u}(q_1)P_R u(p_1)\ \bar{v}(p_2)P_L v(q_2) \\ &\overset{Fierz}{=} -if_{ij}f_{i'j'}\frac{1}{\hat{t} - m_\eta^2}\frac{1}{2}\bar{u}(q_1)\gamma^\mu P_L v(q_2)\ \bar{v}(p_2)\gamma_\mu P_R u(p_1)\ . \end{aligned} \tag{II.35}$$

When $|\hat{t}| \ll m_\eta^2$ we can identify this amplitude as a 4-fermion contact interaction and equate

$$\frac{f_{ij}f_{i'j'}}{2m_\eta^2} = \frac{4\pi}{\Lambda_{LR}^2} \tag{II.36}$$

where Λ_{LR}, with $L\,(R)$ chirality refers to the lepton (quark), is often the limit quoted for the 4-fermion contact interactions. Since only the limits Λ_{LL} are quoted in PDG [23], which was based on Ref. [25], we use the limit of Λ_{LR} obtained in Ref. [25]. The limit on $\Lambda_{LR} \approx 11 - 16$ TeV depending on the sign of the 4-fermion contact interaction. Let us simply take $\Lambda_{LR} = 16$ TeV, and translate into the mass limit of m_η as follows (with $i = i' = 1$ and $j = j' = 1$ or 2) [1]

$$m_\eta \gtrsim f_{1j} \times 3.2 \text{ TeV} \qquad (j = 1, 2)\ . \tag{II.37}$$

The effect of including the $\hat{t}$ or $\hat{u}$ in the leptoquark propagator has been explicitly worked out in Refs. [28, 29]. It was shown that the limits obtained with the proper leptoquark propagators are weakened by about 40% to a few % for leptoqark mass of 1 TeV to 3 TeV. Nevertheless, the direct search limits of around 1 TeV are more restrictive then.

Note that the approximation $1/(\hat{t} - m_\eta^2) \simeq 1/(-m_\eta^2)$ may not be valid for $m_\eta \lesssim 1$ TeV. Yet, the limit obtained in Eq. (II.37) is a rough estimate on how heavy the η boson can be without upsetting the current Drell-Yan data. If the η boson is around 1 TeV, the Drell-Yan invariant-mass distribution may receive some enhancement at the large invariant-mass end.

Similarly, we can write down the amplitudes for $u^c_{L_i}\overline{u^c_{L_{i'}}} \to \ell_{L_j}\bar{\ell}_{L_{j'}}$ and $d^c_{L_i}\overline{d^c_{L_{i'}}} \to \ell_{L_j}\bar{\ell}_{L_{j'}}$ with the exchange of $\delta_{1/3}$ and $\delta_{4/3}$, respectively. The resulting mass limits on m_δ can be written as

$$\frac{g_{1j}g_{1j}}{2m_\delta^2} = \frac{4\pi}{\Lambda_{LL}^2}\ . \tag{II.38}$$

With a more severe $\Lambda_{LL} \approx 25$ TeV, we obtain

$$m_\delta \gtrsim g_{1j} \times 5.0 \text{ TeV} \qquad (j = 1, 2)\ . \tag{II.39}$$

We observe that the mass limit on δ is somewhat stronger than η, simply because of the chiralities of quarks and leptons that they induce.

On the other hand, the η and δ bosons can be directly pair produced by the strong interaction, followed by their decays into leptons and quarks. Therefore, the typical signature would be a pair of leptons and a pair of jets in the final states, of which the invariant mass of one jet and one lepton shows a clear peak. Note that the jets can be light or heavy flavors

[1] The most updated limits by the ATLAS and CMS on the compositeness scale are $\Lambda_\pm(LL) \gtrsim 17 - 25$ TeV (ATLAS) [26] and $11 - 18$ TeV (CMS) [27], which are somewhat less restrictive than the limits that we quoted from the PDG. We therefore used the PDG values. Nevertheless, the limits are not as stringent as the direct search limits of around 1 TeV provided that the values for f_{1j} and g_{1j} are less $O(10^{-1})$.

depending on the Yukawa couplings f_{ij} and g_{ij}, and the leptons can be neutrinos or charged leptons of different or same flavors. The current limits on leptoquarks, using electron or muon plus jets, are about 1 TeV [30]. Pair production cross sections have been calculated with NLO accuracy in Ref. [32] long time ago. The cross section at 13 TeV LHC is of order $O(10)$ fb for 1 TeV η or δ boson. Combining the direct search limit of about 1 TeV for η and δ, and Eqs. (II.37) and (II.39), we obtain upper limits for f_{1j} and g_{1j}:

$$f_{1j} \lesssim 0.3, \qquad g_{1j} \lesssim 0.2 \qquad (j = 1, 2)\ . \tag{II.40}$$

A list of more comprehensive collider and low energy constraints can be found in Ref. [31].

III. $b \to s\bar{\ell}\ell$ ANOMALY AND PREDICTIONS

The more striking anomaly was the lepton-universality violation measured in the ratio $R_K \equiv B(B \to K\mu\mu)/B(B \to Kee) = 0.745^{+0.090}_{-0.074} \pm 0.036$ by LHCb [8], and the less one was the angular distributions of $B \to K^*\mu\mu$ [9]. The new-physics contributions to the effective Hamiltonian characterizing the decay processes are

$$\mathcal{H}^f_{\rm eff} = \frac{f_{b\ell} f_{s\ell'}}{4}\left(\frac{c^2_{\alpha_2}}{m^2_{A_2}} + \frac{s^2_{\alpha_2}}{m^2_{B_2}}\right)\left[(\bar{s}\gamma^\mu P_R b)(\bar{\ell}'\gamma_\mu \ell) - (\bar{s}\gamma^\mu P_R b)(\bar{\ell}'\gamma_\mu\gamma_5 \ell)\right], \tag{III.1}$$

$$\mathcal{H}^g_{\rm eff} = -\frac{g_{b\ell} g_{s\ell'}}{4m^2_\delta}\left[(\bar{s}\gamma^\mu P_L b)(\bar{\ell}'\gamma_\mu \ell) - (\bar{s}\gamma^\mu P_L b)(\bar{\ell}'\gamma_\mu\gamma_5 \ell)\right]. \tag{III.2}$$

Therefore, the relevant new-physics Wilson coefficients for the operators $C^{(\prime)}_{9,10}$ are given by

$$(C'_9)^{\ell\ell'} = \frac{1}{C_{\rm SM}}\frac{f_{b\ell} f_{s\ell'}}{4}\left(\frac{c^2_{\alpha_2}}{m^2_{A_2}} + \frac{s^2_{\alpha_2}}{m^2_{B_2}}\right), \quad (C'_{10})^{\ell\ell'} = -(C'_9)^{\ell\ell'}, \tag{III.3}$$

$$(C_9)^{\ell\ell'} = -(C_{10})^{\ell\ell'} = -\frac{1}{C_{\rm SM}}\frac{g_{b\ell} g_{s\ell'}}{4m^2_\delta}, \quad C_{\rm SM} \equiv \frac{V_{tb}V^*_{ts} G_F \alpha_{\rm em}}{\sqrt{2}\pi}, \tag{III.4}$$

where $\alpha_{\rm em} \approx 1/137$ is the fine-structure constant, and $\mathrm{G_F} \approx 1.17 \times 10^{-5}$ GeV^{-2} is the Fermi constant. In our analysis, we focus on the case of $\ell = \ell' = \mu$ and we write the $\mu\mu$ component simply as $C_9(C_{10})$ and $C'_9(C'_{10})$ in the following. In Table V [10], we summarize the best fit values of the Wilson coefficients for explaining the experimental anomalies where we focus on the cases of $C_9 = -C_{10}$ and $C'_9 = -C'_{10}$ since most of the allowed parameter sets provide either $C_9 \ll C'_9$ or $C_9 \gg C'_9$ as we show in our numerical analysis. Note that $(C_9)^{\mu\mu}$ and $(C'_9)^{\mu\mu}$ are roughly estimated as

$$C_9[C'_9] \sim 3.3 \times 10^2 \left(\frac{1\,\mathrm{TeV}}{m_{LQ}}\right)^2 g_{b\mu} g_{s\mu}[f_{b\mu} f_{s\mu}], \tag{III.5}$$

	Best fit	1σ	3σ
$C_9 = -C_{10}$	-0.68	$[-0.85, -0.50]$	$[-1.22, -0.18]$
$C'_9 = -C'_{10}$	0.19	$[0.07, 0.31]$	$[-0.17, 0.55]$

TABLE V: Summary for the new physics contribution to $C_{9,10}(C'_{9,10})$ explaining experimental anomalies of the $b \to s\bar{\ell}\ell$ processes in the cases of $C_9 = -C_{10}$ and $C'_9 = -C'_{10}$ where new physics contribution is nonzero only for the values on the table for both cases.

where m_{LQ} indicates the leptoquark mass. Therefore, the bi-product of the couplings are required to be $\sim O(10^{-3})$ to obtain the best fit value for $\sim$1 TeV leptoquark mass.

A. Numerical analysis

We are now ready to search for the allowed parameter space, which satisfies all the constraints that we have discussed above, in particular those explaining the $b \to s\mu\mu$ anomalies. First of all, we fix some mass parameters as $m_{A_2} = m_{A_1}$ and $m_{B_2} = m_\delta = m_{B_1}$ where we require degenerate masses for the components of η and Δ to suppress the oblique parameters ΔS and ΔT. We prepare 80 million random sampling points for the relevant input parameters with the following ranges:

$$\begin{aligned} &(m_{A_1}, m_{B_1}) \in [1\,, 5\,]\text{TeV}, \quad |A_{12,23,13}| \in \left[10^{-13},\ 10^{-7}\right] \text{GeV}, \\ &(\alpha_1,\ \alpha_2) \in [10^{-5}, 10^{-2}], \quad |f_{ij}| \in [10^{-5}, 4\pi]. \end{aligned} \tag{III.6}$$

After scanning, we find 709 parameter sets, which can fit neutrino oscillation data and satisfy all the constraints. Note that mixing angle $\alpha_{1(2)}$ is required to be small due to the constraints from ΔS and ΔT parameters.

In the left panel of Fig. 4, we show the allowed region in m_{A_1}-m_{B_1} plane, which suggests the relation $m_{A_1} \lesssim m_{B_1}$ that is mainly required from the constraints of ΔS and ΔT. We also put a vertical line of $m_{A_1} = 1$ TeV onto the figure, because the collider limit on leptoquarks is roughly 1 TeV. In the right panel of Fig. 4, we show the allowed region in C_9-C'_9 plane. It suggests that the relation $C_9(\in [0, 0.2]) \ll C'_9(\in [0, 0.7])$ is realized for most of the parameter region while a parameter set provides $C_9 \sim C'_9$; the cases of $C_9(= -C_{10}) < 0$ and $C'_9(= -C'_{10}) < 0$ are disfavored by the constraints from B_s and B_d decay branching ration Eqs. (II.18) and (II.19). $C_9(= -C_{10}) \sim C'_9(= -C'_{10})$ case is not favored by the global

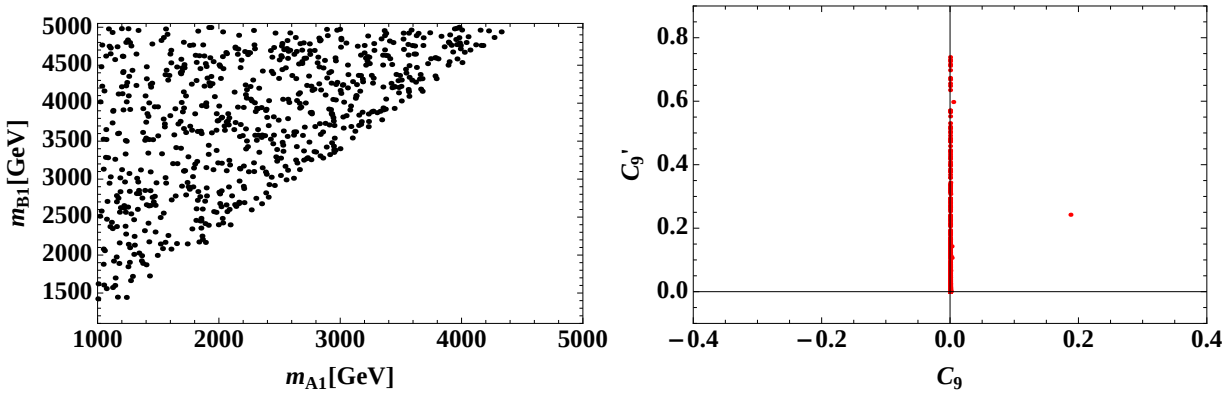

FIG. 4: Scattering plots in the plane of m_{A_1} versus m_{B_1} in the left panel; and in the plane of C_9 versus C_9' in the right panel. The vertical line of 1 TeV is superimposed in the left panel due to the direct search limit of leptoquarks.

analysis. In Fig. 5, we show the scatter plots of $f_{11,12,13}$ versus $m_{A_1} = m_{A_2} \approx m_\eta$ (left panels), and $g_{11,12,13}$ versus $m_{B_1} = m_{B_2} \approx m_\delta$ (right panels). f_{11} and f_{13} go over all the range, while f_{12} is favor of rather larger value. On the other hand, $[g_{11}, g_{12}] \lesssim \mathcal{O}(1)$, while g_{13} is likely to a free parameter, as shown in Fig. 6.

We note that the $\mu \to e\gamma$ process provides the strongest constraint which bounds the combinations of the couplings $|f^\dagger_{2i} f_{i1}|$ and $|g^\dagger_{2i} g_{i1}|$. Therefore, we can see that the collider limits obtained from the Drell-Yan process in Eqs. (II.37) and (II.39) are weaker than the direct search mass limits of leptoquarks (~ 1 TeV).

B. Collider Predictions

The most striking signature of the model is the lepton-flavor violating production via the η or δ bosons in the t-channel, resulting in the final states of $e^\pm\mu^\mp$, $e^\pm\tau^\mp$, or $\mu^\pm\tau^\mp$. The SM irreducible backgrounds to these final states are negligible. Since the δ boson is in general heavier than the η boson, we use the subprocess $d\bar{d} \to \ell_i\ell_j$ via the exchange of the η boson to estimate the event rates. We give the signal event rates in Table VI, using the parameters $f_{11} = 10^{-2}, f_{12} = f_{13} = 10^{-1}$ and $m_\eta = 1$ TeV at the 13 TeV LHC with 300 fb^{-1} luminosity. Naively, the production cross section for $\ell_i\ell_j$ is proportional to $|f_{1i} f_{1j}|^2$. If we choose $f_{11} = 10^{-1}$ instead of 10^{-2} the event rate will increase by 100 times, although the number of parameter points for $f_{11} = 10^{-1}$ is considerably less. Therefore, the event rates

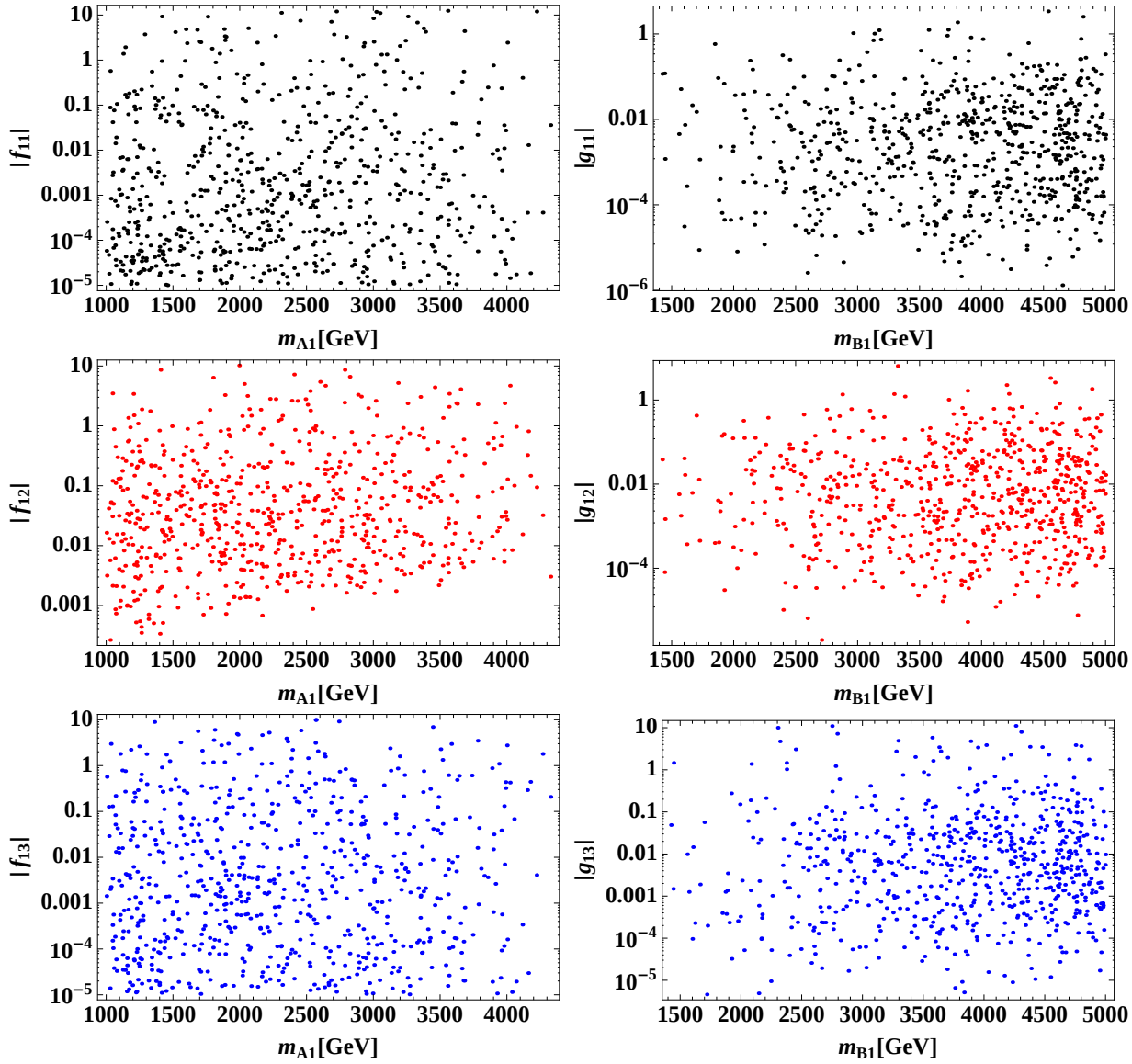

FIG. 5: Scatter plots of f_{1j} versus $m_{A_1} = m_{A_2} \approx m_\eta$ (left panels), and g_{1j} versus $m_{B_1} = m_{B_2} \approx m_\delta$ (right panels). The vertical line of 1 TeV is superimposed due to the direct search limit of leptoquarks.

may be large enough for observation if the Yukawa couplings f_{1j} are of order $O(10^{-1})$.

As we have mentioned above, pair production cross sections for leptoquarks have been calculated with NLO accuracy [32] and the cross sections at 13 TeV LHC for 1 TeV η or δ bosons is of order $O(10)$ fb. The final state consists of two leptons and two jets, among which the corresponding lepton and jet will form an invariant-mass peak. On the other hand, the η or δ bosons can also be singly produced with the subprocess $gq \to \eta\ell$ [33], followed by the

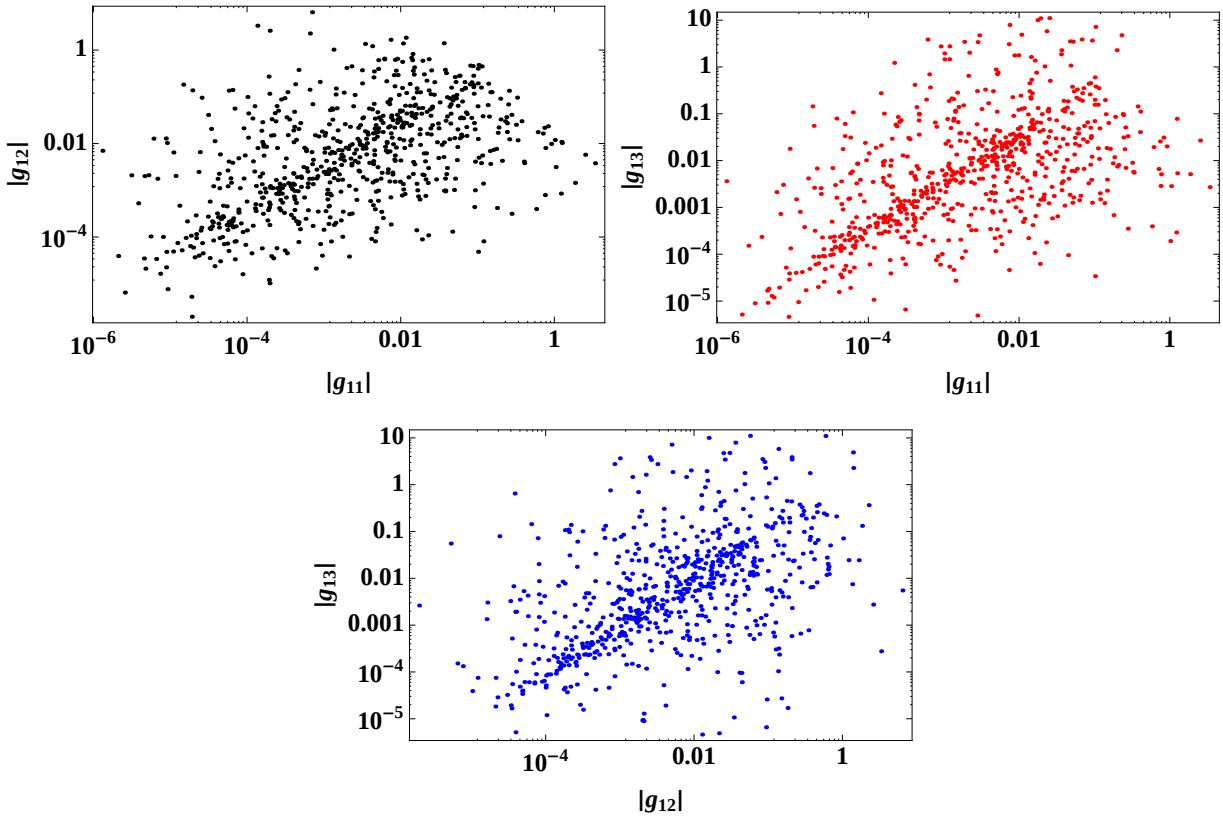

FIG. 6: Scatter plots of g_{11} versus g_{12} with black dots (upper left), g_{11} versus g_{13} with red dots (upper right), and g_{12} versus g_{13} with blue dots (lower). These trends mainly come from $\ell_a \to \ell_b \gamma$ at one-loop level. Especially, the upper left panel (black dotted) is more restrictive than the other two panels, because both components g_{12} and g_{11} are related to the most stringent constraint of $\mu \to e\gamma$.

TABLE VI: Event rates for the $e^\pm\mu^\mp$, $e^\pm\tau^\mp$, or $\mu^\pm\tau^\mp$ final states with exchange of the η boson in the subprocess $d\bar{d} \to e^- e^+$ at the 13 TeV LHC with 300 fb^{-1} luminosity.

Inputs	$e^\pm\mu^\mp$	$e^\pm\tau^\mp$	$\mu^\pm\tau^\mp$
$f_{11} = 10^{-2}$, $f_{12} = f_{13} = 10^{-1}$, $m_\eta = 1$ TeV	0.057	5.7	0.057

decay of η into a lepton and a quark. The amplitude for the production involves a strong coupling and a Yukawa coupling (f_{ij} for η but g_{ij} for δ). Nevertheless, since the sizes of f_{ij} and g_{ij} are very small because of the small neutrino mass, the production cross section for single η or δ is very suppressed. We shall not further consider this production mechanism.

IV. CONCLUSIONS

We have proposed a simple extension of the SM with two leptoquark-like scalar bosons η and Δ, which couple to all three generations of fermions. It can explain the neutrino masses and oscillations data, and the most importantly explain the anomalies observed in $b \to s\ell^+\ell^-$ including the lepton-universality violation and angular distributions, and is at the same time consistent with all the LFVs, FCNCs, Drell-Yan production, and collider searches.

We offer a few more comments as follows.

1. The contributions of η and Δ to the muon $g-2$ are negligible compared to the experimental uncertainties.

2. The contributions of the $\eta_{2/3}$ to the Drell-Yan process, proportional to $|f_{11}|^4$ ($|f_{12}|^4$) for e^+e^- ($\mu^+\mu^-$) final state, will show up as an enhancement in the large invariant-mass region.

3. The most interesting collider signature for the η or δ boson is the lepton-flavor violating production such as $e^\pm\mu^\mp$, $e^\pm\tau^\mp$, and $\mu^\pm\tau^\mp$, which are proportional to $|f_{11}f_{12}|^2$, $|f_{11}f_{13}|^2$, and $|f_{12}f_{13}|^2$, respectively. The event rates may be large enough for observation if the Yukawa couplings f_{1j} are of order $O(10^{-1})$.

4. The direct search limits on η or δ bosons, just like leptoquarks, are currently stronger than the indirect bounds from the Drell-Yan process that we obtained in Eqs. (II.37) and (II.39).

Acknowledgments

This work was supported by the Ministry of Science and Technology of Taiwan under Grants No. MOST-105-2112-M-007-028-MY3.

Appendix A: New particle contributions to vacuum polarization diagram

Here we summarize the contributions to $\Pi_\pm(q^2)$, $\Pi_{33}(q^2)$, $\Pi_{3Q}(q^2)$ and $\Pi_{QQ}(q^2)$ in Eq. (II.32) and (II.33) from new particles in our model.

Contributions to $\Pi_\pm(q^2)$

The one loop contributions from three-point gauge interaction are denoted by $\Pi_\pm^{XY}(q^2)$ where X and Y indicate the particles inside the loop. They are summarized as follows;

$$\Pi_\pm^{A_1(B_1)\delta_{4/3}}(q^2) = \frac{2}{(4\pi)^2} s_{\alpha_1}^2 (c_{\alpha_1}^2) G(q^2, m_{A_1(B_1)}^2, m_\delta^2), \tag{A.1}$$

$$\Pi_\pm^{B_1\delta_{4/3}}(q^2) = \frac{2}{(4\pi)^2} c_{\alpha_1}^2 G(q^2, m_{B_1}^2, m_\delta^2), \tag{A.2}$$

$$\Pi_\pm^{A_1A_2}(q^2) = \frac{2}{(4\pi)^2} \left(s_{\alpha_1} s_{\alpha_2} - \frac{1}{\sqrt{2}} c_{\alpha_1} c_{\alpha_2} \right)^2 G(q^2, m_{A_1}^2, m_{A_2}^2), \tag{A.3}$$

$$\Pi_\pm^{B_1B_2}(q^2) = \frac{2}{(4\pi)^2} \left(c_{\alpha_1} c_{\alpha_2} - \frac{1}{\sqrt{2}} s_{\alpha_1} s_{\alpha_2} \right)^2 G(q^2, m_{B_1}^2, m_{B_2}^2), \tag{A.4}$$

$$\Pi_\pm^{A_1B_2}(q^2) = \frac{2}{(4\pi)^2} \left(s_{\alpha_1} c_{\alpha_2} + \frac{1}{\sqrt{2}} c_{\alpha_1} s_{\alpha_2} \right)^2 G(q^2, m_{A_1}^2, m_{B_2}^2), \tag{A.5}$$

$$\Pi_\pm^{B_1A_2}(q^2) = \frac{2}{(4\pi)^2} \left(c_{\alpha_1} s_{\alpha_2} - \frac{1}{\sqrt{2}} s_{\alpha_1} c_{\alpha_2} \right)^2 G(q^2, m_{B_1}^2, m_{A_2}^2), \tag{A.6}$$

where

$$\begin{aligned} G(q^2, m_P^2, m_Q^2) &= \int dxdy\delta(1-x-y)\Delta_{PQ}[\Upsilon + 1 - \ln \Delta_{PQ}], \\ \Delta_{PQ} &= -q^2 x(1-x) + xm_P^2 + ym_Q^2, \quad \Upsilon = \frac{2}{\epsilon} - \gamma - \ln(4\pi). \end{aligned} \tag{A.7}$$

The one loop contributions from four-point gauge interaction are denoted by $\Pi_\pm^X(q^2)$ where X indicates the particle inside the loop. They are summarized as follows;

$$\Pi_\pm^{A_1}(q^2) = -\frac{1}{2(4\pi)^2} (4s_{\alpha_1}^2 + c_{\alpha_1}^2) H(m_{A_1}^2), \tag{A.8}$$

$$\Pi_\pm^{A_2}(q^2) = -\frac{1}{2(4\pi)^2} (2s_{\alpha_2}^2 + c_{\alpha_2}^2) H(m_{A_2}^2), \tag{A.9}$$

$$\Pi_\pm^{B_1}(q^2) = -\frac{1}{2(4\pi)^2} (4c_{\alpha_1}^2 + s_{\alpha_1}^2) H(m_{B_1}^2), \tag{A.10}$$

$$\Pi_\pm^{B_2}(q^2) = -\frac{1}{2(4\pi)^2} (2c_{\alpha_2}^2 + s_{\alpha_2}^2) H(m_{B_2}^2), \tag{A.11}$$

$$\Pi_\pm^{\delta_{4/3}}(q^2) = -\frac{1}{(4\pi)^2} H(m_\delta^2), \tag{A.12}$$

where

$$H(m_P^2) = m_P^2[\Upsilon + 1 - \ln m_P^2]. \tag{A.13}$$

Contributions to $\Pi_{33}(q^2)$, $\Pi_{3Q}(q^2)$ and $\Pi_{QQ}(q^2)$

The one loop contributions from three-point gauge interaction are denoted by $\Pi_{33,3Q,QQ}^{XY}(q^2)$

where X and Y indicate particles inside the loop. They are summarized as follows;

$$\Pi^{A_1A_1}_{[33,3Q,QQ]} = \frac{2}{(4\pi)^2}\left[\frac{1}{4}c^4_{\alpha_1}, \frac{1}{6}c^2_{\alpha_1}, \frac{1}{9}\right] G(q^2, m^2_{A_1}, m^2_{A_1}), \tag{A.14}$$

$$\Pi^{B_1B_1}_{[33,3Q,QQ]} = \frac{2}{(4\pi)^2}\left[\frac{1}{4}s^4_{\alpha_1}, \frac{1}{6}s^2_{\alpha_1}, \frac{1}{9}\right] G(q^2, m^2_{B_1}, m^2_{B_1}), \tag{A.15}$$

$$\Pi^{A_1B_1}_{[33,3Q,QQ]} = \frac{2}{(4\pi)^2}\left[\frac{1}{4}s^2_{\alpha_1}c^2_{\alpha_1}, 0, 0\right] G(q^2, m^2_{A_1}, m^2_{B_1}) \tag{A.16}$$

$$\Pi^{A_2A_2}_{[33,3Q,QQ]} = \frac{2}{(4\pi)^2}\left[s^4_{\alpha_2} - s^2_{\alpha_2}c^2_{\alpha_2} + \frac{1}{4}c^4_{\alpha_2}, \frac{2}{3}s^4_{\alpha_2} - s^2_{\alpha_2}c^2_{\alpha_2} + \frac{1}{3}c^4_{\alpha_2}, \frac{4}{9}(s^2_{\alpha_2} - c^2_{\alpha_2})^2\right] G(q^2, m^2_{A_2}, m^2_{A_2}), \tag{A.17}$$

$$\Pi^{B_2B_2}_{[33,3Q,QQ]} = \frac{2}{(4\pi)^2}\left[c^4_{\alpha_2} - s^2_{\alpha_2}c^2_{\alpha_2} + \frac{1}{4}s^4_{\alpha_2}, \frac{2}{3}c^4_{\alpha_2} - s^2_{\alpha_2}c^2_{\alpha_2} + \frac{1}{3}s^4_{\alpha_2}, \frac{4}{9}(s^2_{\alpha_2} - c^2_{\alpha_2})^2\right] G(q^2, m^2_{B_2}, m^2_{B_2}), \tag{A.18}$$

$$\Pi^{A_2B_2}_{[33,3Q,QQ]} = \frac{2}{(4\pi)^2}s^2_{\alpha_2}c^2_{\alpha_2}\left[\frac{9}{4}, 3, 4\right] G(q^2, m^2_{A_2}, m^2_{B_2}), \tag{A.19}$$

$$\Pi^{\delta_{4/3}\delta_{4/3}}_{[33,3Q,QQ]} = \frac{2}{(4\pi)^2}\left[1, \frac{4}{3}, \frac{16}{9}\right] G(q^2, m^2_{\delta}, m^2_{\delta}). \tag{A.20}$$

The one loop contributions from four-point gauge interaction are denoted by $\Pi^X_{33,3Q,QQ}(q^2)$ where X indicates the particle inside the loop. They are summarized as follows;

$$\Pi^{A_1}_{[33,3Q,QQ]} = -\frac{2}{(4\pi)^2}\left[s^2_{\alpha_1} + \frac{1}{4}c^2_{\alpha_1}, \frac{2}{3}s^2_{\alpha_1} + \frac{1}{6}c^2_{\alpha_1}, \frac{4}{9}s^2_{\alpha_1} + \frac{1}{9}c^2_{\alpha_1}\right] H(m^2_{A_1}), \tag{A.21}$$

$$\Pi^{B_1}_{[33,3Q,QQ]} = -\frac{2}{(4\pi)^2}\left[c^2_{\alpha_1} + \frac{1}{4}s^2_{\alpha_1}, \frac{2}{3}c^2_{\alpha_1} + \frac{1}{6}s^2_{\alpha_1}, \frac{4}{9}c^2_{\alpha_1} + \frac{1}{9}s^2_{\alpha_1}\right] H(m^2_{B_1}), \tag{A.22}$$

$$\Pi^{A_2}_{[33,3Q,QQ]} = -\frac{2}{(4\pi)^2}\left[\frac{1}{4}c^2_{\alpha_2}, \frac{1}{3}c^2_{\alpha_2}, \frac{1}{9}s^2_{\alpha_2} + \frac{4}{9}c^2_{\alpha_2}\right] H(m^2_{A_2}), \tag{A.23}$$

$$\Pi^{B_2}_{[33,3Q,QQ]} = -\frac{2}{(4\pi)^2}\left[\frac{1}{4}s^2_{\alpha_2}, \frac{1}{3}s^2_{\alpha_2}, \frac{1}{9}c^2_{\alpha_2} + \frac{4}{9}s^2_{\alpha_2}\right] H(m^2_{B_2}), \tag{A.24}$$

$$\Pi^{\delta_{4/3}}_{[33,3Q,QQ]} = -\frac{2}{(4\pi)^2}\left[1, \frac{4}{3}, \frac{16}{9}\right] H(m^2_{\delta}). \tag{A.25}$$

[1] R. N. Mohapatra and G. Senjanovic, Phys. Rev. Lett. **44**, 912 (1980). doi:10.1103/PhysRevLett.44.912

[2] A. Ibarra, E. Molinaro and S. T. Petcov, JHEP **1009**, 108 (2010) doi:10.1007/JHEP09(2010)108 [arXiv:1007.2378 [hep-ph]].

[3] F. del Aguila and J. A. Aguilar-Saavedra, Nucl. Phys. B **813**, 22 (2009) doi:10.1016/j.nuclphysb.2008.12.029 [arXiv:0808.2468 [hep-ph]].

[4] A. Zee, Phys. Lett. B **93**, 389 (1980) Erratum: [Phys. Lett. B **95**, 461 (1980)]. doi:10.1016/0370-2693(80)90349-4, 10.1016/0370-2693(80)90193-8

[5] E. Ma, Phys. Rev. D **73**, 077301 (2006) doi:10.1103/PhysRevD.73.077301 [hep-ph/0601225].

[6] A. Zee, Nucl. Phys. B **264**, 99 (1986), K. S. Babu, Phys. Lett. B **203**, 132 (1988).

[7] L. M. Krauss, S. Nasri and M. Trodden, Phys. Rev. D **67**, 085002 (2003) doi:10.1103/PhysRevD.67.085002 [hep-ph/0210389].

[8] R. Aaij *et al.* [LHCb Collaboration], Phys. Rev. Lett. **113**, 151601 (2014) doi:10.1103/PhysRevLett.113.151601 [arXiv:1406.6482 [hep-ex]].

[9] R. Aaij *et al.* [LHCb Collaboration], Phys. Rev. Lett. **111**, 191801 (2013) [arXiv:1308.1707 [hep-ex]].

[10] S. Descotes-Genon, L. Hofer, J. Matias and J. Virto, JHEP **1606**, 092 (2016) [arXiv:1510.04239 [hep-ph]].

[11] G. Hiller and M. Schmaltz, Phys. Rev. D **90**, 054014 (2014) doi:10.1103/PhysRevD.90.054014 [arXiv:1408.1627 [hep-ph]].

[12] G. Hiller, D. Loose and K. Schonwald, arXiv:1609.08895 [hep-ph].

[13] Z. Maki, M. Nakagawa and S. Sakata, Prog. Theor. Phys. **28**, 870 (1962). doi:10.1143/PTP.28.870

[14] D. V. Forero, M. Tortola and J. W. F. Valle, Phys. Rev. D **90**, no. 9, 093006 (2014) doi:10.1103/PhysRevD.90.093006 [arXiv:1405.7540 [hep-ph]].

[15] T. Nomura and H. Okada, arXiv:1609.01504 [hep-ph].

[16] M. Carpentier and S. Davidson, Eur. Phys. J. C **70**, 1071 (2010) [arXiv:1008.0280 [hep-ph]].

[17] S. Chatrchyan *et al.* [CMS Collaboration], Phys. Rev. Lett. **111**, 101804 (2013) [arXiv:1307.5025 [hep-ex]].

[18] R. Aaij *et al.* [LHCb Collaboration], Phys. Rev. Lett. **111**, 101805 (2013) [arXiv:1307.5024 [hep-ex]].

[19] S. Sahoo and R. Mohanta, Phys. Rev. D **91**, no. 9, 094019 (2015) [arXiv:1501.05193 [hep-ph]].

[20] A. M. Baldini *et al.* [MEG Collaboration], arXiv:1605.05081 [hep-ex].

[21] J. Adam *et al.* [MEG Collaboration], Phys. Rev. Lett. **110**, 201801 (2013) [arXiv:1303.0754 [hep-ex]].

[22] F. Gabbiani, E. Gabrielli, A. Masiero and L. Silvestrini, Nucl. Phys. B **477**, 321 (1996) doi:10.1016/0550-3213(96)00390-2 [hep-ph/9604387].

[23] K.A. Olive et al. (Particle Data Group), Chin. Phys. C, 38, 090001 (2014) and 2015 update.

[24] T. Mandal, S. Mitra and S. Seth, Phys. Rev. D **93**, no. 3, 035018 (2016) doi:10.1103/PhysRevD.93.035018 [arXiv:1506.07369 [hep-ph]].

[25] K. m. Cheung, Phys. Lett. B **517**, 167 (2001) [hep-ph/0106251].

[26] ATLAS Collaboration, EXO Summary for ICHEP 2016: *https://twiki.cern.ch/twiki/bin/view/AtlasPublic/ExoticsPublicResults#Exotics_summary_plots*

[27] CMS Collaboration, EXO Summary for ICHEP 2016: *https://twiki.cern.ch/twiki/bin/view/CMSPublic/PhysicsResultsEXO*

[28] A. Bessaa and S. Davidson, Eur. Phys. J. C **75**, no. 2, 97 (2015) doi:10.1140/epjc/s10052-015-3313-0 [arXiv:1409.2372 [hep-ph]].

[29] S. Davidson, S. Descotes-Genon and P. Verdier, Phys. Rev. D **91**, no. 5, 055031 (2015) doi:10.1103/PhysRevD.91.055031 [arXiv:1410.4798 [hep-ph]].

[30] See for example, M. Aaboud *et al.* [ATLAS Collaboration], New J. Phys. **18**, no. 9, 093016 (2016) [arXiv:1605.06035 [hep-ex]].

[31] I. Dorsner, S. Fajfer, A. Greljo, J. F. Kamenik and N. Kosnik, Phys. Rept. **641**, 1 (2016) doi:10.1016/j.physrep.2016.06.001 [arXiv:1603.04993 [hep-ph]].

[32] M. Kramer, T. Plehn, M. Spira and P. M. Zerwas, Phys. Rev. D **71**, 057503 (2005) [hep-ph/0411038].

[33] T. Mandal, S. Mitra and S. Seth, JHEP **07**, 028 (2015) [arXiv:1503.04689 [hep-ph]].